mathematics

MDPI

Article

Fatigue Characteristics of Long-Span Bridge-Double Block Ballastless Track System

Bin Yan [1,2], Jianghao Tian [1], Jie Huang [3,*] and Ping Lou [1]

[1] School of Civil Engineering, Central South University, Changsha 410075, China
[2] National Engineering Research Center of High-Speed Railway Construction Technology, Changsha 410075, China
[3] CSCEC AECOM Consultants Co., Ltd., Lanzhou 730000, China
* Correspondence: jiehuang0203@126.com

Abstract: The key issues in designing ballastless track for high-speed railway bridges are to reduce maintenance and improve track smoothness by understanding fatigue damage characteristics. This paper is based on the principle of bridge-rail interaction and train-track-bridge coupling dynamics, the refined simulation model of bridge-CRTS I Bi-block ballastless track system is established by using the finite element method. The longitudinal force distribution law of CWR (Continuously Welded Rail) and the dynamic response characteristics of coupling systems are studied, based on the Miner rule and S-N curve. The fatigue characteristics of ballastless track system laying on long-span bridge under the dynamic train load and the effect of ballastless track system design parameters changes on fatigue characteristics are discussed. The results show that the extreme values of longitudinal force of CWR all appear in the middle of the bridge span or near the bridge bearing, and attention should be paid to the strength checking of CRW laying on long-span bridge. Under the dynamic train load, the fatigue life curve of rail on the bridge is relatively smooth and the minimum life of rail which is laying on continuous bridge decreases from 27.1 years to 17 years that which is laying on cable-stayed bridge. The life curve of track plate laying on continuous bridge is relatively smooth, and the life curve of track plate laying on cable-stayed bridge is related to the stiffness of elastic cushion, which decreases in a stepped manner, and there will be no fatigue failure on the track plate during service. The life curve of the baseplate is related to the type of bridge, the minimum life value of the baseplate appears near the bridge bearing, and there will be no fatigue failure on the baseplate during service. Increasing the stiffness of elastic cushion can effectively improve the fatigue life of track plate, and increasing the vertical stiffness of fasteners can enhance the connection between rail and track plate and improve the fatigue life of rail. The increase in train speed will increase the dynamic stress amplitude of track structure and reduce the fatigue life of the rail.

Keywords: track engineering; ballastless track; continuous bridge; long-span cable-stayed bridge; S-N curves; fatigue characteristic

MSC: 37N15

Citation: Yan, B.; Tian, J.; Huang, J.; Lou, P. Fatigue Characteristics of Long-Span Bridge-Double Block Ballastless Track System. *Mathematics* **2023**, *11*, 1792. https://doi.org/10.3390/math11081792

Academic Editors: Chuangyin Dang and Siyang Gao

Received: 2 March 2023
Revised: 27 March 2023
Accepted: 7 April 2023
Published: 9 April 2023

1. Introduction

Due to the facts of the relatively soft structure system of large-span cable-stayed bridge and its large bridge curvature and beam end angle, domestic and foreign high-speed railway large-span cable-stayed bridge girder has often been laid with a ballast track structure in recent years. Compared with ballastless track, ballast track is low in operation ride comfort and durability, the road bed maintenance workload is large, and the operation management and maintenance cost are high. Poor track quality can result in a negative impact on the interaction between trains and infrastructure [1], as well as a decline in passenger comfort [2]. In order to unify the whole line track form, to render

uniform transition stiffness and to improve the line quality, it is of great significance to study the adaptability and fatigue durability characteristics of the ballastless track system on the long-span bridge.

At present, domestic and foreign researchers have made a deep study on the interaction between the bridge and the ballastless track on the bridge under the temperature load and the train vertical load and under the action of braking load [3–6], The fatigue characteristics of ballastless track on subgrade and simple supported beam are preliminarily discussed. Relevant research results have definite significance for enriching the ballastless track theory and for guiding the engineering practice, For example, Xu Qingyuan et al. [7] established the vertical connecting plate ballastless track model on a simple branch beam bridge of high-speed railway, The cracking and closing effect of ballastless track concrete cracks are considered and the life of ballastless track structure in Wuhan, Harbin and Guangzhou is predicted. Zhu Zhihui et al. [8] built the vehicle-bridge dynamics model of 64 m steel truss bridge based on the vehicle-bridge coupling vibration theory and the influence of different train types and running speed on bridge fatigue damage is analyzed. Li Shiyun et al. [9] takes CRTS I-type plate ballastless track as their research object and, considering the fatigue characteristics of the ballastless track structure on the subgrade under the combined action of train load and ambient temperature, concluded that during the service of ballastless track, given there was little fatigue damage from rail plate, base plate and convex retaining platform, CA mortar needs to be strengthened in maintenance during the service. Shaanxi Yao et al. [10] studied, in the context of typical soft soil areas, the damage characteristics of track plate under the action of uneven subgrade settlement, train load and temperature field. They point out that the uneven settlement of subgrade is the key factor causing the track plate damage, The limit value of uneven settlement of subgrade is also given. Ren Juanjuan et al. [11] relying on passenger and cargo common line railway CRTS I type plate ballastless track, predicted the life of the oris plate under different loads. Elisa Poveda et al. [12], by using the digital signal processing method, where the frequency amplitude was assigned a random phase, selected the most unfavorable cases from a large number of measured train load combinations. Based on this load operating condition, compression damage to the rail plate was assessed, and suggestions to optimize the fatigue life of the rail plate were made.

The existing research on the fatigue damage of ballastless track mainly focuses on roadbed or simply supported beams. The fatigue damage characteristics of the ballastless track system on long-span bridge are not clear. In this paper, based on experimental data and relevant classical literature, a (40 + 64 + 40) m continuous beam on Beijing-Shenyang passenger special line and a 300-m mixed beam cable-stayed bridge on Chang-Jiangxi passenger special line are taken as the research object, and the simulation model of bridge-CRTS I type double block ballastless track is established by using the finite element method. The longitudinal force distribution law of seamless line on bridge and dynamic response characteristics of bridge, track bed plate, base plate and rail under train live load were studied. Combined with Miner's rule and S-N curve, the fatigue damage law of ballastless track structure on long-span bridge under train load was discussed. The influence of elastic cushion stiffness, fastener stiffness and train running speed on the fatigue characteristics of ballastless track structure is revealed.

2. Simulation Model of Double Block Ballastless Track System on Bridge

2.1. Ballastless Track Structure

The rail is CHN60 rail, and the fastener is the WJ-8B type fastener. The vertical stiffness of the fastener is 35 kN/mm. The fastener system includes small resistance fasteners and normal resistance fasteners. The relation between the longitudinal displacement of the rail relative to the rail bearing platform and the longitudinal resistance of fastener is [13]

$$r_1 = \begin{cases} 11.625x & |x| \leq 2\ \text{mm} \\ 23.25\text{sign}(x) & |x| > 2\ \text{mm} \end{cases} \quad (1)$$

$$r_2 = \begin{cases} 12.4x|x| \leq 0.5 \text{ mm} \\ 6.2\text{sign}(x)|x| > 0.5 \text{ mm} \end{cases} \quad (2)$$

wherein, r_1 is the longitudinal resistance of the normal resistance fastener (kN); r_2 is the longitudinal resistance of the low resistance fastener (kN); x is the longitudinal displacement of the rail relative to the rail bearing platform (mm).

The expression of the relation between transverse deformation and resistance of fasteners is

$$r_3 = \begin{cases} 4.5x|x| \leq 2 \text{ mm} \\ 9\text{sign}(x)|x| > 2 \text{ mm} \end{cases} \quad (3)$$

wherein, r_3 is the transverse resistance of the fastener (kN); x is the transverse displacement of the rail relative to the rail bearing platform (mm).

Each end of the cable-stayed bridge is provided with one rail expansion regulator (a total of four groups). Apart from the normal resistance fasteners used in the regulator range, the small resistance fasteners are used on the cable-stayed bridge. The fastener on continuous beam bridge adopts constant resistance fastener.

The CRTS I type double block ballastless track structure (Figure 1) on the bridge adopts C40 concrete, and the track bed plate and the base plate are laid in blocks. There are two limit grooves between each road bed plate and the base plate, and the elastic cushion plate is placed around the limit grooves. The height of the bed plate is 240 mm. The height of the base plate in other positions is 260 mm except 290 mm in the scope of the telescopic regulator at both ends of the cable-stayed bridge. The length and width of both the bed plate and the base plate are 5920 × 2800 mm.

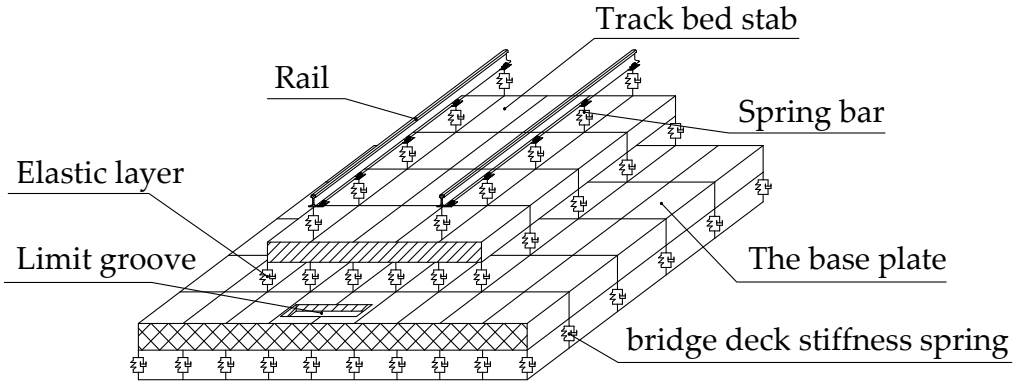

Figure 1. Schematic diagram of CRTS I double block Ballastless track model on the bridge.

The elastic cushion layer is set between the track bed plate and the base plate, and the longitudinal and transverse values of the elastic cushion layer are 91 kN/mm [14]. The vertical stiffness of the elastic cushion layer on the continuous beam bridge is 0.1 N/mm^3, and the elastic cushion stiffness on the cable-stayed bridge is a step transition (Figure 2). The vertical stiffness of the plane support decreases step by step from 0.1 N/mm^3 to 0.025 N/mm^3 and then increases to 0.1 N/mm^3. The stiffness of elastic cushion plate around the limit groove is simulated by nonlinear spring. The stiffness along the bridge is 14.3 kN/mm, and the stiffness across the bridge is 9.8 kN/mm. When the relative displacement between the bed plate and the base plate exceeds the thickness of the elastic cushion, the stiffness along the elastic cushion and the transverse bridge is 10,000 kN/mm. The base plate and the beam body are connected by shear nails, and the bridge deck stiffness spring with a stiffness of 10,000 kN/mm is used for the simulation, so that the base plate and the bridge form a whole.

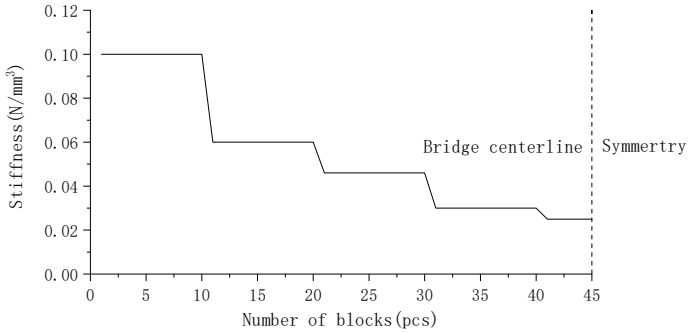

Figure 2. Stiffness of elastic cushion plate on cable-stayed bridge.

2.2. Continuous Beam Structure and Finite Element Model

The beam body of simple supported beam adopts a 32 m prestressed concrete simple supported box girder of double line ballastless track, as shown in Figure 3.

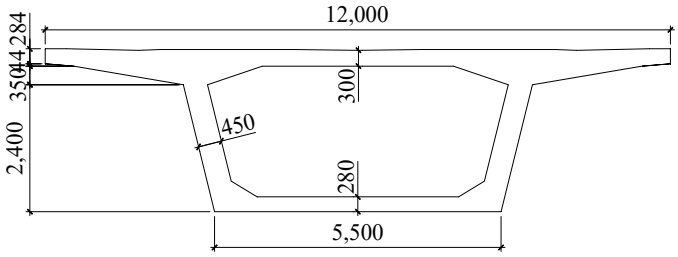

Figure 3. Cross Section Diagram of simply supported box girder (Unit: mm).

The continuous beam adopts a (40 + 64 + 40) m continuous beam on the Beijing-Shenyang passenger special line, and the beam section at the beam end, mid-span and support, as shown in Figure 4.

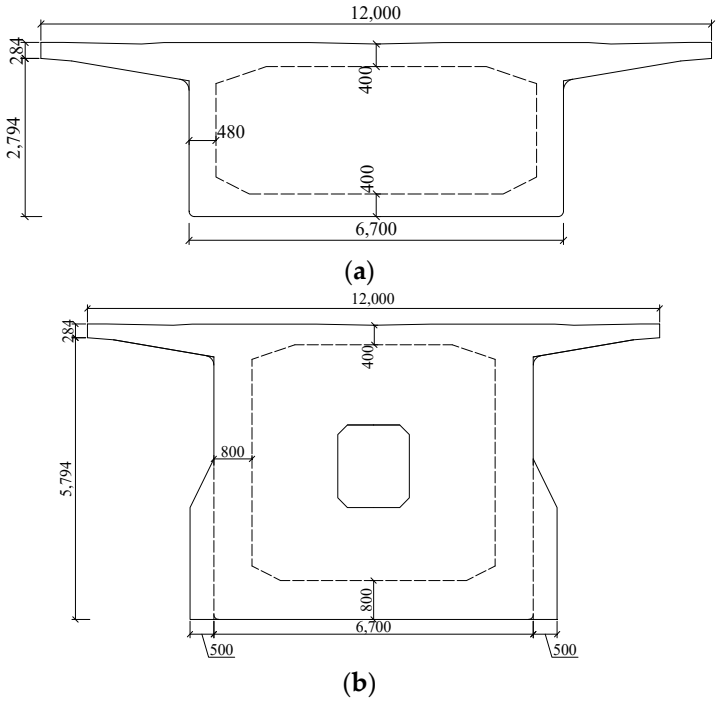

Figure 4. Cross-section diagram of continuous beam (Unit: mm): (**a**) End and mid-span sections of continuous beams; (**b**) section at the support of continuous beam.

According to the section properties of the section at the beam end and the support, the linear interpolation method is used to simulate the section properties of the gradient section from the support to the continuous beam span. The longitudinal stiffness of the pier at the fixed support of the continuous beam and 500 kN/cm at the fixed support of the simple beam are taken as 1000 kN/cm.

The integrated spatial analysis model of continuous beam-CRTS Type I double block ballastless track fully considers the nonlinear constraints of bridge, support, base plate, track bed plate, fastener, rail and other components and structure layers. The steel rail, track bed plate, base plate and beam body are simulated by a beam element, and the connection modes of fastener and elastic cushion are simulated by a nonlinear spring element. Linear spring elements were used to simulate the vertical stiffness of fasteners, elastic cushion, shear nails and bridge support stiffness. Subgrade sections of 100 m were considered at both ends of the simply-supported beam. The finite element model of a continuous beam ballastless track system is shown in Figure 5.

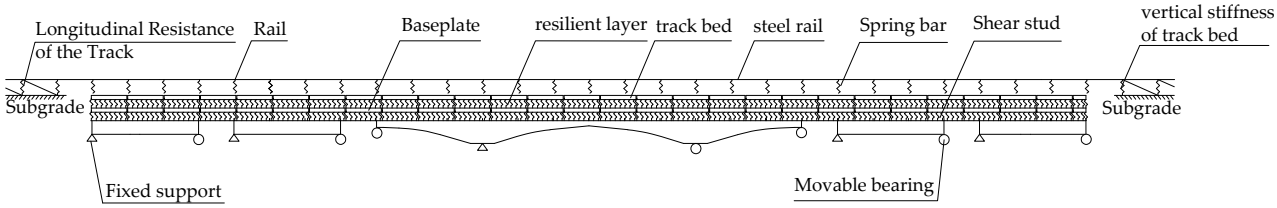

Figure 5. Schematic diagram of a continuous beam ballastless track system model.

The overall damping of the model is Rayleigh damping, the damping ratio h is 0.05, and the damping coefficients α and β are respectively

$$\alpha = 2h\frac{\omega_1\omega_2}{\omega_1+\omega_2}, \beta = 2h\frac{1}{\omega_1+\omega_2} \quad (4)$$

where ω_1 and ω_2 are the first two frequencies that contribute the most to the vertical mode of the structure.

2.3. Structure and Finite Element Model of Cable-Stayed Bridge

The design of the cable-stayed bridge adopts the semi-floating structure system with two towers and two cable planes in space. The initial cable force is exerted by the fan-shaped galvanized cable. The hole span layout of the bridge is (35 + 40 + 60 + 300 + 60 + 40 + 35) m, as shown in Figure 6.

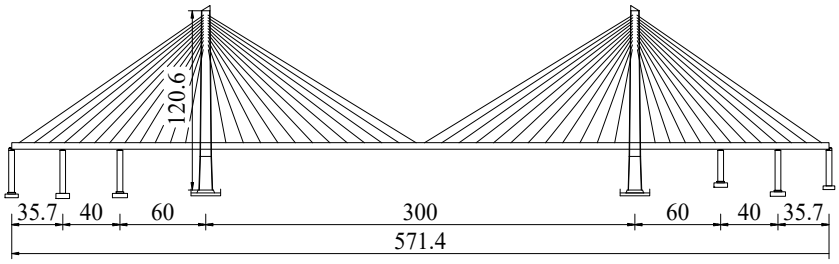

Figure 6. Hole span Layout of cable-stayed bridge (Unit: m).

The bridge tower adopts a large radius curve concrete tower, a longitudinal herring-bone shape, and a transverse single column shape. The height of the two towers is 120.6 m, and a hollow section is adopted to reduce the weight of the towers. Two beams are set on the bridge tower (Figure 7), and an upper beam is set at 31.2 m (herringbone fork) from the top of the tower, with a height of 2.9 m; a lower beam is set at 102.4 m from the top of the tower (bridge deck), with a height of 5 m. A hydraulic viscous damper is set between the

bridge tower and the main beam to withstand wind- and rain-induced vibration, ground motion and other dynamic loads.

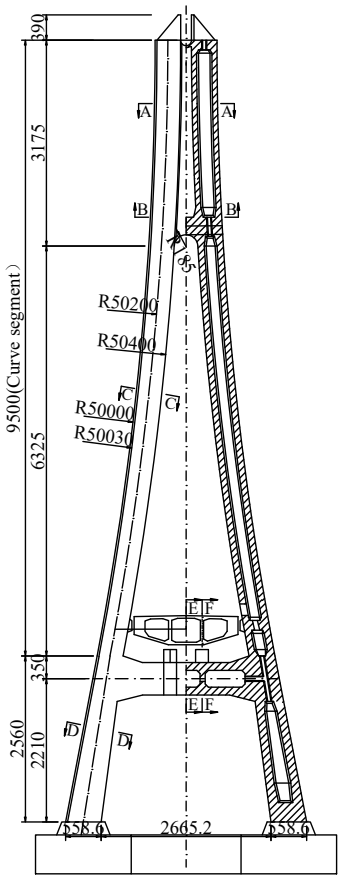

Figure 7. Structure of the cable-stayed tower (Unit: cm).

The side span of the bridge is concrete box girder, which adopts a single-box-and-three-chambers equal section. The top width of the bridge deck is 16.5 m, and the beam at the center is 4.5 m high. The standard cross section has an air nozzle. The side span concrete beam enhances the anchorage effect on the main span and improves the structural stiffness. The 300-m main span is a box-shaped steel-mixed beam with light weight and large span [15]. The top width of the bridge deck is 16.3 m, the height of the center beam is 4.5 m, and the thickness of the concrete bridge panel is 0.3 m and partially thickened to 0.5 m. The main beam structure of cable-stayed bridge is shown in Figure 8.

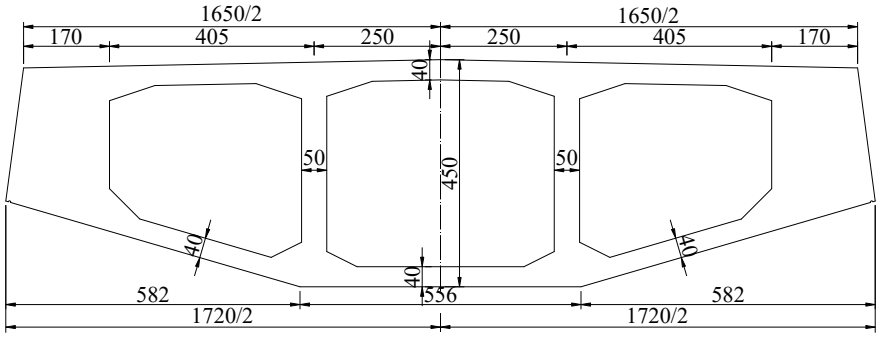

(a)

Figure 8. *Cont.*

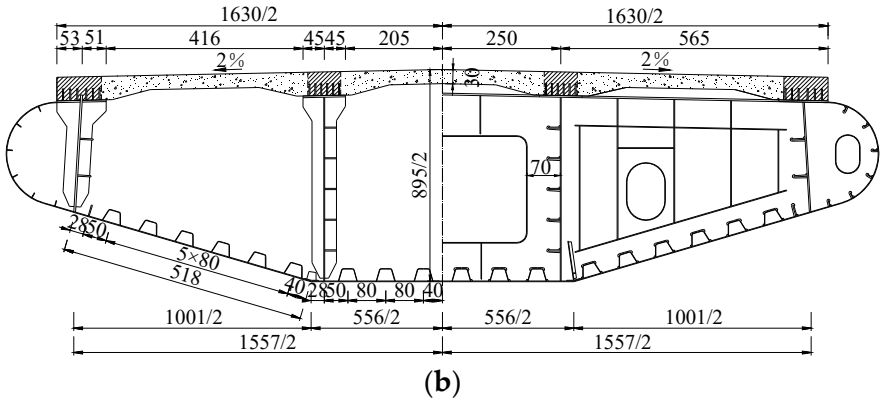

Figure 8. Main beam structure (Unit: cm): (**a**) Side span concrete box girder; (**b**) main span box steel—composite beam.

The integrated spatial analysis model of cable-stayed bridge-CRTS Type I double block ballastless track fully considers the nonlinear constraints between the bridge tower, cable, beam body, support, shear nails, base plate, elastic cushion, track plate, fasteners, rail and other components, as well as the structure layer. Among them, the steel rail, track bed plate, base plate and bridge beam unit are simulated. Linear spring elements were used to simulate the vertical stiffness of fastener, elastic cushion, shear nails, damping support between cable tower and main beam, and stiffness of bridge support. The cable stayed cable was simulated by a tie rod element. The overall damping of the model was Rayleigh damping (Equation (3)). Figure 9 shows the finite element model of the cable-stayed bridge bBallastless track system.

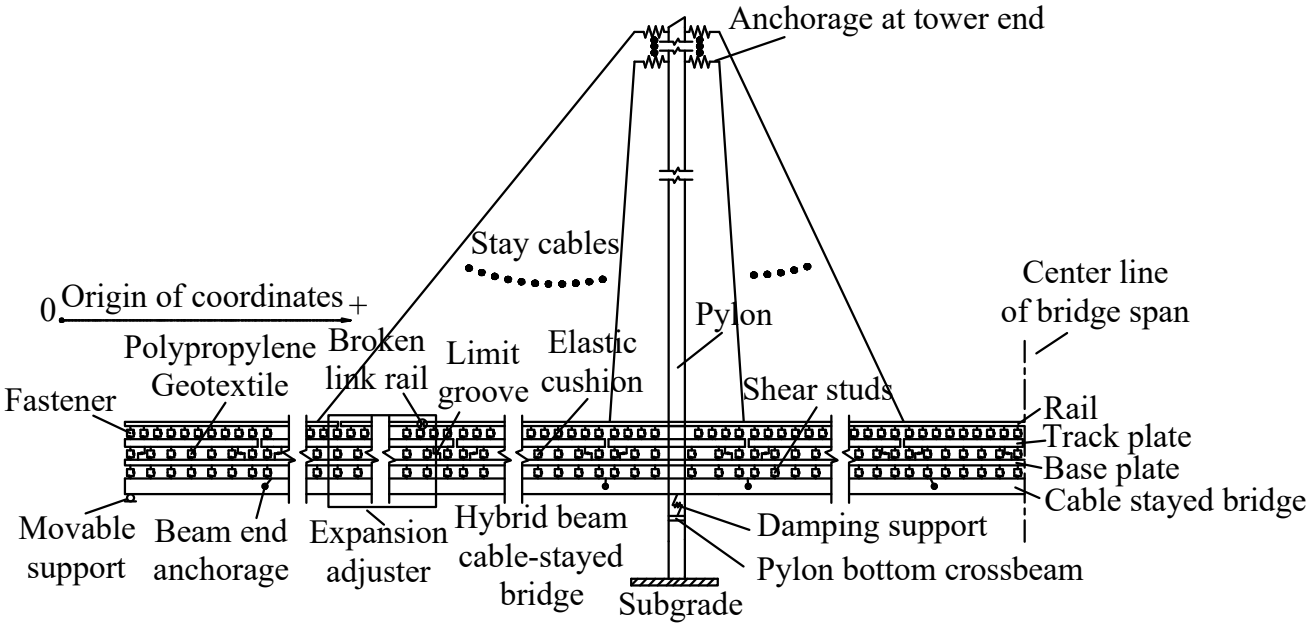

Figure 9. Schematic diagram of the cable-stayed bridge ballastless track system.

2.4. Finite Element Model Verification

In this paper, the fishbone spur model is used to simulate the simple supported beam, continuous beam and cable-stayed bridge, a rigid arm is used to simulate the spatial position of the base plate and support, and a spring unit is used to simulate the constraints between the bridge, the base plate, the track plate and the rail. Based on this modeling method, a calculation example of a single-span single-line 60 m simply-supported beam (in Appendix C.2 of UIC 774-3) is established, and the temperature rise of the beam body

is considered as 35 °C when calculating the expansion force. Braking force is determined according to a 20 kN/m value, with full span loading; the beam end rotates under the action of deflection, and the relative longitudinal displacement from the upper edge of the beam end to the abutment is 8 mm. The calculated results are compared with UIC example C.2, as shown in Table 1.

Table 1. Comparison between calculation results and UIC examples.

Item	Expansion Force			Flexural Force			Braking Force		
	UIC	Example	Error	UIC	Example	Error	UIC	Example	Error
Track stress at fixed support (MPa)	8.00	7.83	2.13%	30.60	30.71	0.36%	28.00	27.36	2.29%
Track stress at sliding support (MPa)	−26.00	−25.62	1.46%	−10.80	−10.29	4.72%	−28.00	−27.83	0.61%

The calculation results are in good agreement with the UIC example, in which the error of flexural force is 4.72%. This is because the analytical algorithm is used in UIC, and the finite element method is used in this paper, so there will be some errors in the results. However, the error is small, which proves that the modeling method used in this paper can correctly simulate the interaction between beams and rails. Moreover, the longitudinal additional force of rail calculated in this paper accords with the general distribution law of longitudinal force of seamless line on long-span bridge [16]. The maximum displacements of 32 m simple supported beam and rail under train load calculated in this paper are 1.8 mm and 0.8 mm respectively, which are larger than the maximum displacements of 32 m simple supported beam and rail under train load in the literature [17], which are 1.1 mm and 0.7 mm respectively. This is because the train running speed in the reference is 250 km/h, while the train running speed in this paper is 350 km/h. As the calculation results are limited by the train load value, analysis method and parameter values of each component in the model, the calculation results in this paper are basically consistent with the results in the reference. To sum up, the bridge-CRTS I double block ballastless track model established in this paper is correct.

3. Calculation Method of Fatigue Life of Ballastless Track Structure

3.1. Calculation Method of Fatigue Life of Ballastless Track Structure

The fatigue failure of the bridge ballastless track system under train load is a high-cycle fatigue problem, and the damage in the structure is mainly cumulative fatigue damage. For such problems, the fatigue life evaluation method based on S-N equation and Miner's Rule is generally used in engineering practice. Therefore, this method is selected as the method to evaluate the fatigue characteristics of the ballastless track structure on the bridge.

For a ballastless track structure, the stress cycle times and stress amplitude under train load can be calculated by rain-flow method. Combined with Miner's rule and S-N curve of materials, the structural damage under multi-stage cyclic stress can be obtained. When the sum of damage numbers reaches a certain critical value (according to Miner's rule, the critical value is usually 1), that is, when $D \geq 1$ is satisfied, fatigue failure of the structure can be assumed

$$D = \sum_i D_i = \sum_i \frac{n_i}{N_{ij}} \tag{5}$$

where, D_i is the damage number at the stress level S_i; n_i is the actual number of cycles of the specimen under stress S_i; N_{ij} is the number of failure cycles of specimen under stress S_i.

For the rail structure, the S-N curve of the welding position of 60 kg/m rail obtained by Japan Railway Research Institute [18] is adopted in this paper. The Miner group method is adopted, and the expression is shown in Equation (5).

$$S = a - blgN \tag{6}$$

where: S is the bending stress amplitude of the rail (MPa); N is the number of cycles required for the rail to reach failure. a and b represent the coefficient of S-N curve obtained by the experiment. When the failure probability is 0.01%, a is 472.01 and b is 48.08.

For concrete structures, the Tepfer single logarithmic tensile S-N fatigue equation is used

$$\frac{\sigma_{max}}{f_i} = 1 - b\left(1 - \frac{\sigma_{max}}{\sigma_{min}}\right)lgN \tag{7}$$

where, b is the reduction coefficient of tensile fatigue strength, which is 0.0611 [7]. ft is the axial tensile strength of concrete under static load. Considering that the ballastless track structure is in a flexural and tensile state under train load, the flexural tensile strength of concrete is about 1.5–2 times of the axial tensile strength [19], 1.5 is taken in this paper. σmax and σmix are the maximum and minimum values of concrete stress respectively. N is the fatigue life of concrete.

3.2. Traffic Load Spectrum

High-speed train vehicles are mainly CRH series high-speed trains, and there is no corresponding standard fatigue car stipulated in the design specifications of Chinese railway Bridges. The medium-live load of railway bridge design specifications [20] is no longer applicable to the design and calculation of structural fatigue strength under dynamic load. The dynamic calculation uses CRH3 series high-speed bullet trains, and some train parameters are shown in the literature [21].

According to the railway track design specification [22], the axle load is 1.5 times static load, and the traffic load of high-speed train is shown in Figure 10. Considering that the passenger carrying weight of high-speed train is small, and that the weight of bullet train and trailer is basically the same, eight trains are used.

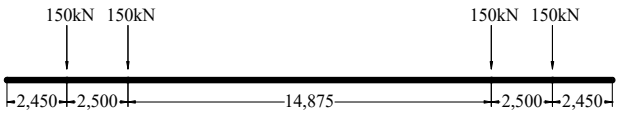

Figure 10. Traffic load spectrum (Unit: mm).

4. Fatigue Characteristics of Continuous Beam-CRTS I Double Block Ballastless Track System

4.1. Additional Stress of Seamless Rail on Continuous Beam Bridge

In order to study the interaction law of large-span continuous beam-rail, the longitudinal additional force of the continuous-beam ballastless track model is calculated, mainly for the expansion force, flexural force and braking force of the confined structure rail. According to the design specification of railway seamless line [23], when calculating the expansion force, the temperature rise of the beam body is set at 30 °C. In the calculation of flexion force, because the concentrated load has little influence on the calculation of additional force, only the vertical uniform load is considered, which is 64 kN/m [16]. The loading length is 300 m according to the train weight divided by the uniform load value. The braking force rate is usually calculated by the wheel-rail adhesion coefficient, which is usually taken as 0.164 in Chinese specifications. The calculation method stipulated in German and UIC specifications is converted to the wheel-rail adhesion coefficient of 0.25. For the sake of safety, the adhesion coefficient of this paper is set at 0.25. When calculating braking force, the longitudinal load is set at 16 kN/m [16] and the loading length is set at 300 m. Flexural and braking loads are shown in Figure 11.

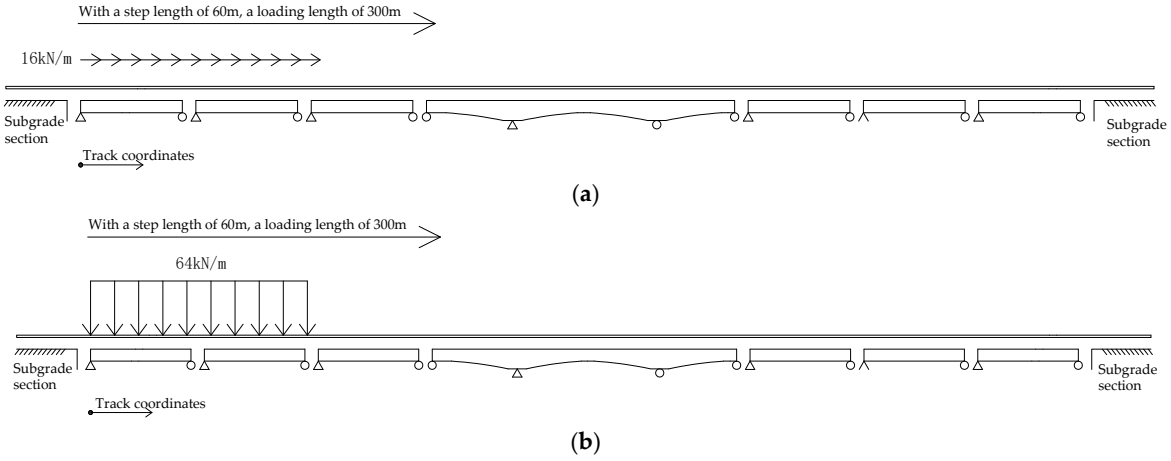

Figure 11. Schematic diagram of loading under load conditions: (**a**) Schematic diagram of flexural force loading; (**b**) Braking force loading diagram.

According to the above calculation conditions, the envelope of rail expansion force, flexural force and braking force is shown in Figure 12.

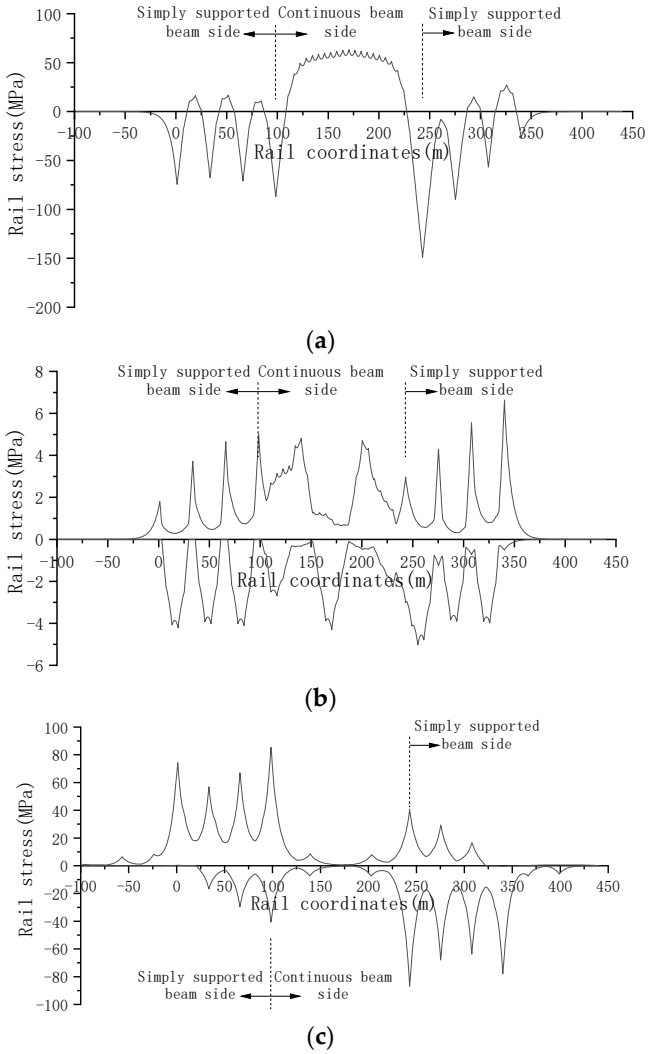

Figure 12. Additional force envelope diagram of seamless rail on continuous beam bridge: (**a**) rail expansion stress; (**b**) rail flexural stress; (**c**) rail braking stress.

As can be seen from Figure 12, the maximum compressive stress of the rail structure of the ballastless track system on the bridge is about 143.1 MPa, which is located at both ends of the simply-supported beam and the continuous beam. The maximum tensile stress is about 61.1 MPa, which appears in the span of the simply-supported beam and the continuous beam. The maximum flexural tensile stress of the rail is about 6.6 MPa near the supports of the simply supported beam and the continuous beam, and the maximum compressive stress is about 5.0 MPa near the middle span of the bridge. The extreme tensile and compressive stresses of rail braking force appear near the supports of simply supported beam and continuous beam, and the extreme tensile and compressive stresses of simply supported beam are much larger than those of continuous beam, with a maximum tensile stress of 85.4 MPa and a maximum compressive stress of 86.8 MPa.

4.2. Dynamic Characteristics of Ballastless Track Structural System on Continuous Beam Bridge

The live load spectrum of the vehicle adopted the traffic load spectrum described in Section 3.2. The running speed of the train was set at 350 km/h, and the integral step of the nonlinear time history was set at 0.005 s. The structural displacements of ballastless track in the middle span of simply supported beam and continuous beam are shown in Figure 13.

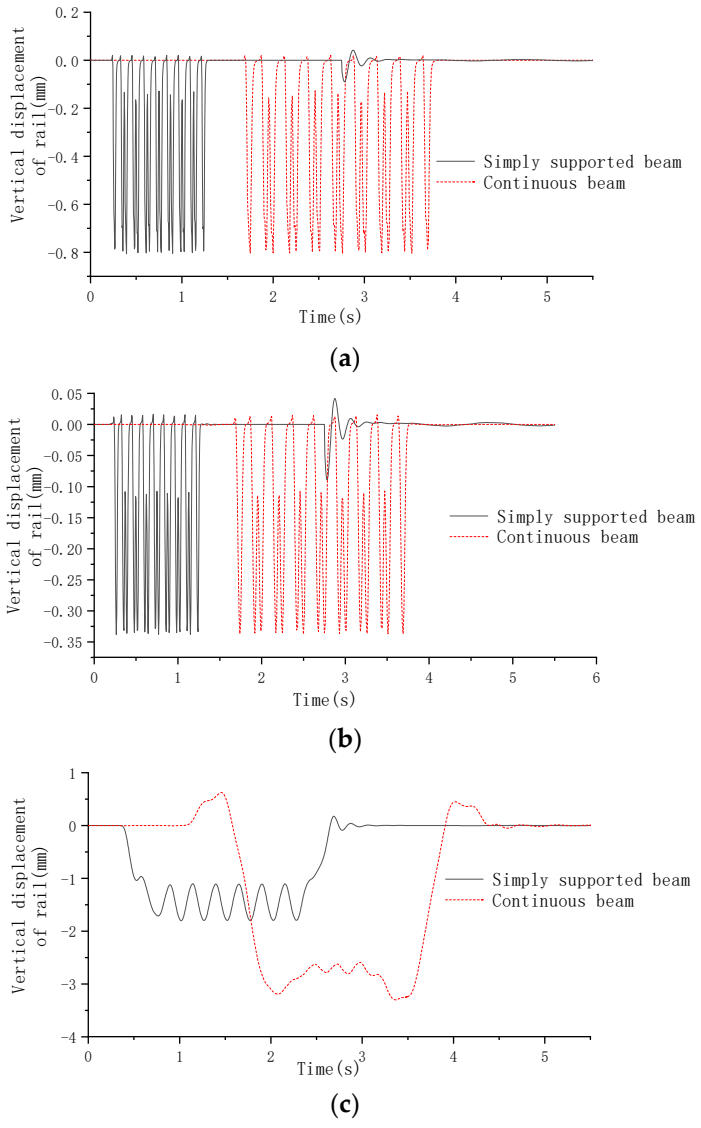

Figure 13. Dynamic displacement of Bridge-Ballastless track system (Unit: mm): (**a**) rail displacement; (**b**) displacement of track bed plate; (**c**) beam displacement.

As can be seen from Figure 13, under the action of train dynamic load, the maximum displacement of rail and track bed plate at the mid-span position of simply supported beam and continuous beam is basically the same, and the bridge structure type has little influence on the dynamic displacement of track structure. For the track structure on the same bridge, the vertical displacement of rail and track bed plate are 0.8 mm and 0.3 mm respectively. Because the span of the continuous beam is larger and softer than that of the simple supported beam, the vertical displacement at the middle span of the continuous beam is larger than that at the middle span of the simple supported beam. The maximum vertical displacement at the middle span of the continuous beam is 3.1 mm and that at the middle span of the simple supported beam is 1.8 mm, with an increase of about 72%.

The stress curves of rail, track plate and base plate at typical positions under the action of train dynamic load are shown in Figure 14.

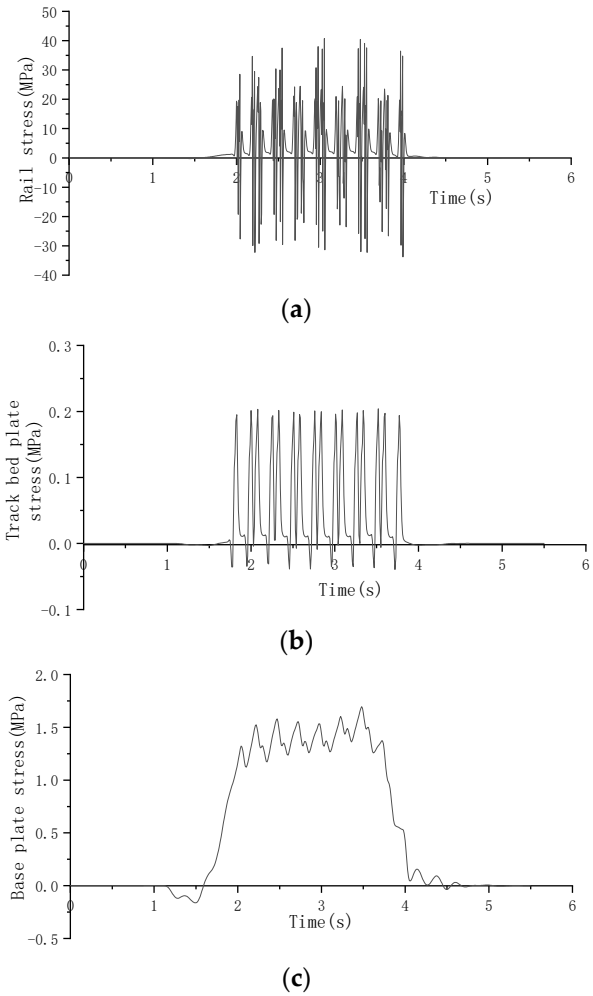

Figure 14. Dynamic stress of rail: (**a**) time history curve of rail stress; (**b**) Stress time history curve of road bed plate; (**c**) Stress time history curve of base plate at the position of middle pier support of continuous beam.

As can be seen from Figure 14, 8 groups of stress cycles with basically the same regularity occur in rail and track bed plate under train load. The maximum tensile and compressive stresses of rail are 40.7 MPa and 33.7 MPa, respectively, and the maximum tensile stress of track bed plate is 0.2 MPa. Due to the flexural deformation of the continuous beam in the span under the action of train load, the beam body near the pier is strained. Accordingly, the tensile stress of the upper base plate is larger, but the compressive stress

is smaller. The maximum tensile stress of the base plate at the support position of the continuous beam pier reaches 1.7 MPa.

4.3. Fatigue Characteristics of Ballastless Track System on Continuous Beam Bridge

It is assumed that 220 trains pass through each day. Based on the fatigue life calculation method of ballastless track structure described in Section 3.1, the fatigue life curve of rail on continuous beam bridge and the fatigue life curve at the most unfavorable position of each track bed plate and base plate are obtained, as shown in Figure 15.

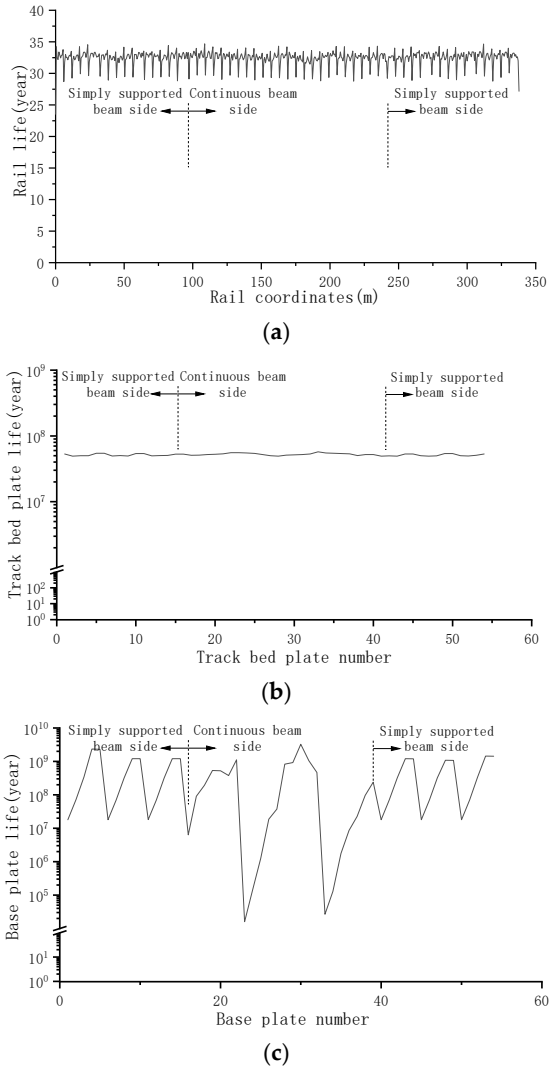

Figure 15. Fatigue life of ballastless track structure on continuous beam: (**a**) rail fatigue life; (**b**) Fatigue life of bed plate; (**c**) Fatigue life of base plate.

As can be seen from Figure 15, the life curve of rail and track bed plate on simply supported beam and continuous beam is smooth, and the life is essentially the same. The life of rail at the most unfavorable position is 27.1 years, but the track bed plate will not suffer fatigue damage during service. As the base plate is consolidated with the beam surface through shear nails, its fatigue life is related to the bridge. The bridge bends under the action of train load in the middle span, and the base plate on it has a larger compressive stress and a smaller tensile stress due to the bending pressure, so the life of the base plate in the middle span is longer. The bending in the span of the bridge will elongate the bridge near the pier, which will cause the tension of the base plate near the pier support, so the life of the base plate near the pier is slightly shorter. The service life of the base plate in

the middle span of the bridge is longer, and the service life of the base plate near the pier support is slightly shorter. The fatigue failure of the base plate will not occur during the service period.

Compared with the simple supported beam, the span of the continuous beam is larger, the structural system pair is softer, and the vertical displacement of the continuous beam under the action of train load is larger than that of the simple supported beam. Therefore, the life of the base plate at the main pier support of the continuous beam is smaller than that at the pier support of the simple supported beam.

5. Fatigue Characteristics of Cable Stayed Bridge CRTS I Double Block Ballastless Track System

5.1. Additional Stress of CWR Rail on Cable-Stayed Bridge

In order to study the interaction law between beam and rail of long-span cable-stayed bridge, the longitudinal additional force of the cable-stayed bridge ballastless track model is calculated, mainly for the calculation of expansion force, deflection force and braking force of the restricted structure rail. Under the action of temperature load, the temperature of side span concrete beam rises by 30 °C and the temperature of main span steel-concrete composite beam rises by 50 °C, and the rail expansion force is calculated. The vertical load of high-speed railway train is 64 kN/m, the loading length is 300 m, and the rail bending force is calculated. The train braking load is 16 kN/m, the loading length is 300 m, and the braking force is calculated. The envelope diagram of additional force of jointless rail on bridge is shown in Figure 16.

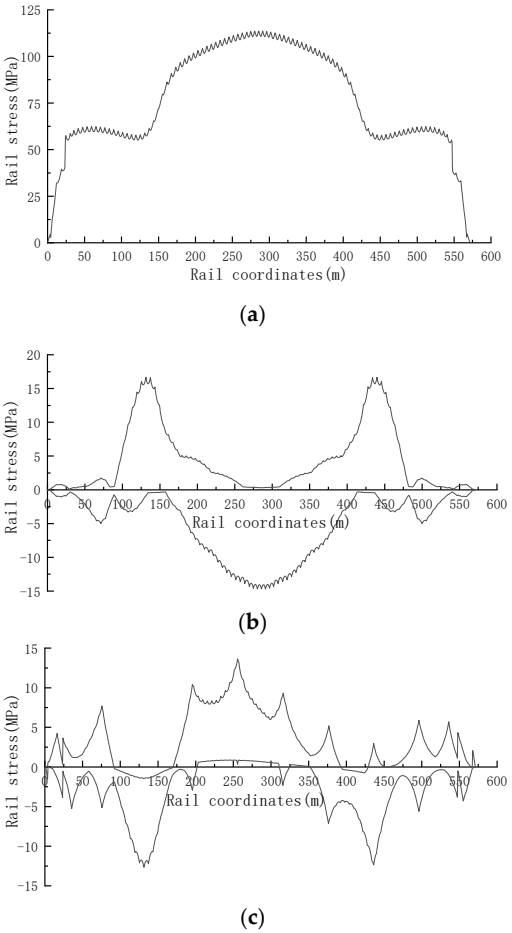

Figure 16. Envelope Diagram of Additional Force of CWR Rail on Cable Stayed Bridge: (**a**) rail expansion and compression stress; (**b**) rail bending stress; (**c**) rail braking stress.

As we can see in Figure 16, as the temperature load on the mid span beam is greater than that on the side span beam, the maximum expansion and compression stress of the rail occurs in the mid span of the main beam, reaching 112.8 MPa; The extreme value of steel rail bending tensile stress appears near the bridge tower support, which is 16.6 MPa, and the steel rail tensile stress in the middle of the main beam span is close to 0; The extreme value of the bending compressive stress of the rail appears in the middle of the main beam span, which is 14.6 MPa; The maximum braking tensile stress of the steel rail occurs in the middle of the main beam span, which is 13.6 MPa, and the maximum braking compressive stress occurs near the bridge tower support, which is 12.6 MPa.

5.2. Dynamic Characteristics of Ballastless Track System on Cable-Stayed Bridge

The live load of the vehicle adopts the load spectrum in Section 3.2, the train speed is 350 km/h, and the nonlinear time integration step is 0.005 s. The dynamic response time history curve of ballastless track system on cable-stayed bridge is calculated, as shown in Figure 17.

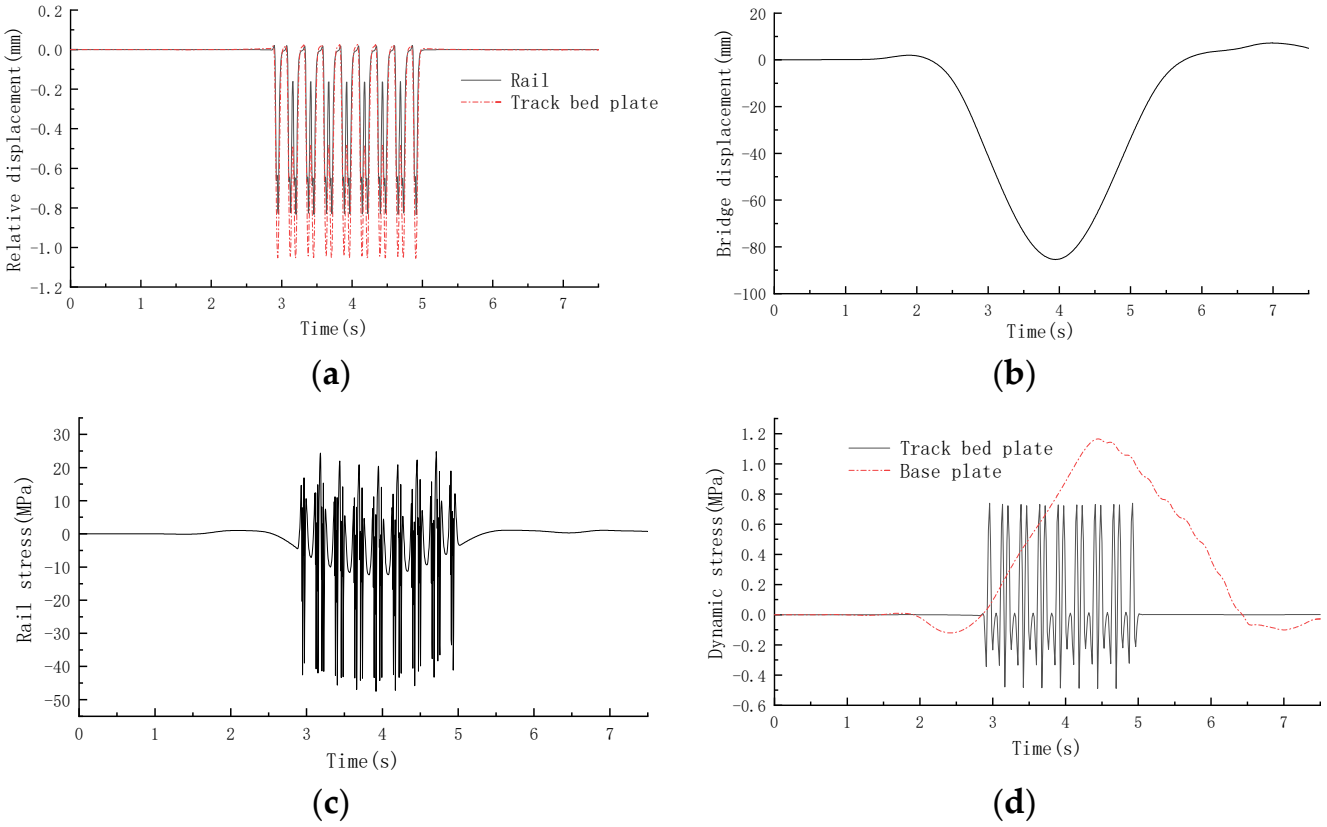

Figure 17. Time history curve of dynamic response of ballastless track system: (**a**) vertical relative displacement in midspan; (**b**) vertical displacement of main beam midspan; (**c**) dynamic stress of mid span steel rail; (**d**) mid span dynamic stress of structure.

From Figure 17 it can be seen that there are 8 cycles for vertical displacement of rail and track bed slab structure, and the maximum relative displacement is not more than 1.0 mm; The maximum vertical displacement in the middle of the main beam of the cable-stayed bridge is 87.5 mm; The cable tower of the cable-stayed bridge is equipped with damping bearings, so the vertical displacement of the main beam near the tower is small, 2.8 mm; The maximum tensile and compressive stresses in the rail stress cycle are 24.4 MPa and 47.5 MPa respectively; The maximum tensile stress of the track bed plate in the middle of the main beam span occurs at the center of the plate bottom, which is 0.74 MPa. The base

plate bottom at the bridge tower support is under tension, and the maximum tensile stress is 1.15 MPa.

5.3. Fatigue Characteristics of Ballastless Track System on Cable-Stayed Bridge

Assuming that the daily throughput of trains is 220, based on the fatigue life calculation method of ballastless track structure described in Section 3.1, the fatigue life curve of steel rails on cable-stayed bridges and the fatigue life curve at the most unfavorable position of each track bed plate and base plate are obtained, as Figure 18 showed.

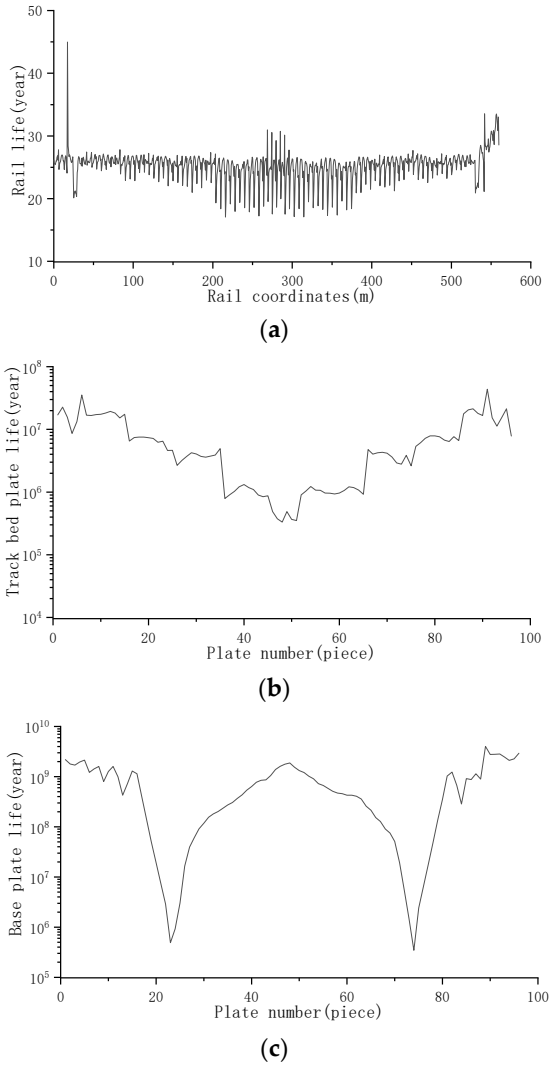

Figure 18. Time history curve of dynamic response of ballastless track system: (**a**) Fatigue life of rail; (**b**) Fatigue life of track bed slab; (**c**) Fatigue life of base plate.

In Figure 18 it can be seen that the rail life curve is relatively smooth. The shortest service life is 17 years in the middle of the bridge span, and the shortest service life is 20 years in the side span, which is 1.17 times of that in the middle span. As the vertical stiffness of the elastic cushion surface support on the cable-stayed bridge decreases step by step from both ends of the bridge to the middle of the span, the service life of the track bed slab decreases step by step from both ends of the bridge to the middle, and the track bed slab will not suffer fatigue damage during its service life. There is an active damping support between the cable tower and the main beam, so the life of the base plate at the bridge tower support is relatively small, and the base plate will not be fatigue damaged during the service period.

6. Influence of Key Parameters of Ballastless Track System on Fatigue Characteristics

Based on the simulation model of double block ballastless track of cable-stayed bridge CRTS I established previously, this section mainly studies the influence of changes in elastic cushion stiffness, fastener stiffness and train speed on the fatigue characteristics of the ballastless track system on the bridge.

6.1. Stiffness of Elastic Cushion

The elastic damping cushion under the slab is set on the long-span cable-stayed bridge, which can support its upper track bed plate structure, disperse the train load, and coordinate the force transmission and deformation between ballastless track and steel-concrete composite beam. To discuss the influence of different elastic damping cushion stiffness on the fatigue life of ballastless track when the train speed is 350 km/h, as Figure 19 showed.

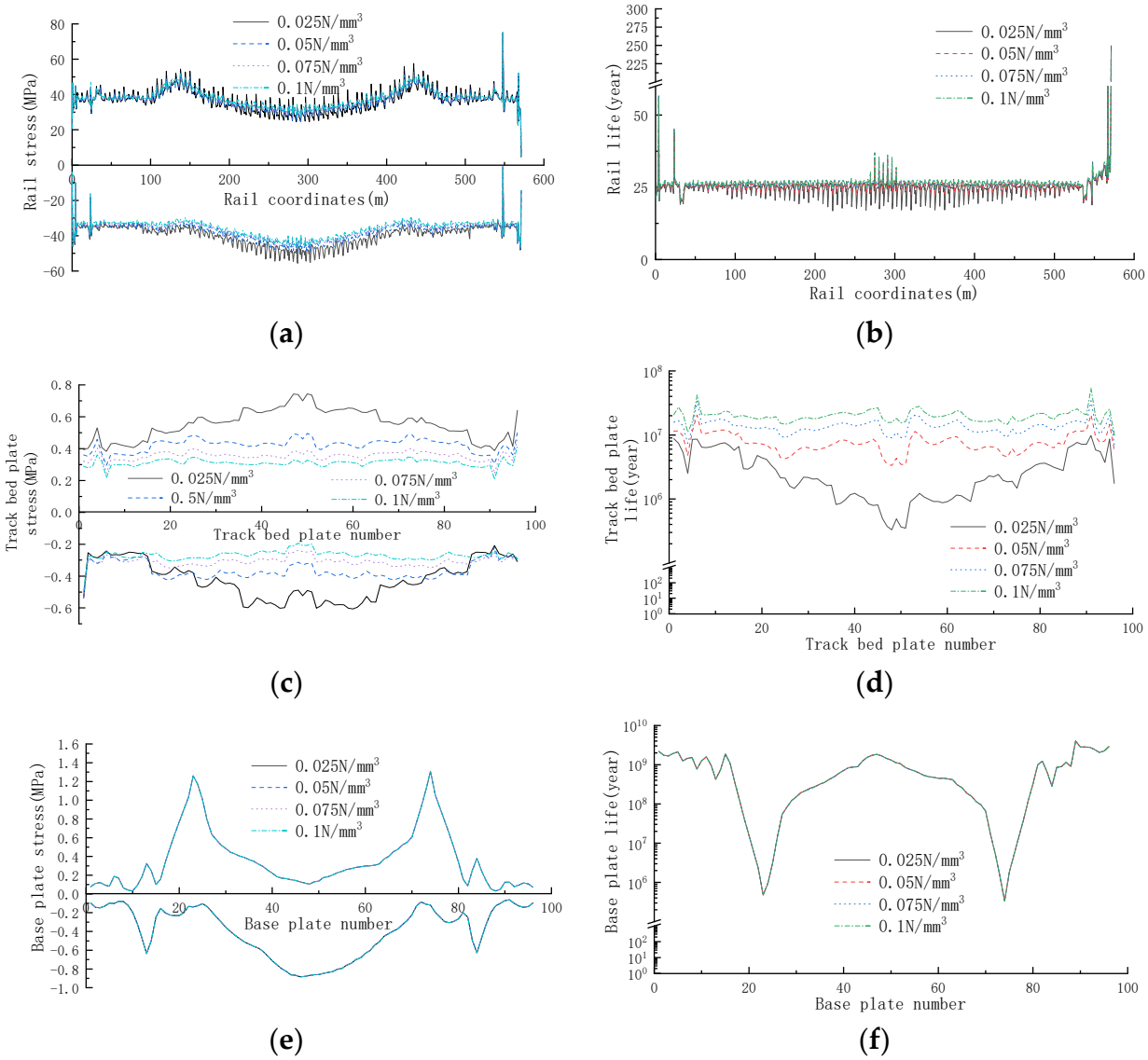

Figure 19. Fatigue characteristics of structures with different elastic cushion stiffness: (**a**) stress envelope diagram of rail; (**b**) rail fatigue life; (**c**) stress envelope diagram of track bed slab; (**d**) fatigue life of track bed slab; (**e**) stress envelope diagram of base plate; (**f**) fatigue life of base plate.

It can be seen from Figure 19 that, as to rail structure, with an increase in elastic cushion stiffness, the rail stress and rail life change slightly, as the maximum tensile and compressive stresses of the track bed slab decrease, and the life of the track bed slab at the most unfavorable position increases from 3.3×10^5 years to 9.9×10^6 years. This is because, with the increase in stiffness, the relative displacement between the track bed plate and the base plate under the action of train load decreases, and so the tensile and compressive stress of the track bed plate decreases, and thus the service life of the track bed plate increases. The tensile and compressive stresses and the minimum life of the base plate are basically unchanged.

6.2. Vertical Stiffness of Fastener

The fatigue characteristics of the structure under different fastener vertical stiffness when the train speed is 350 km/h are shown in Figure 20.

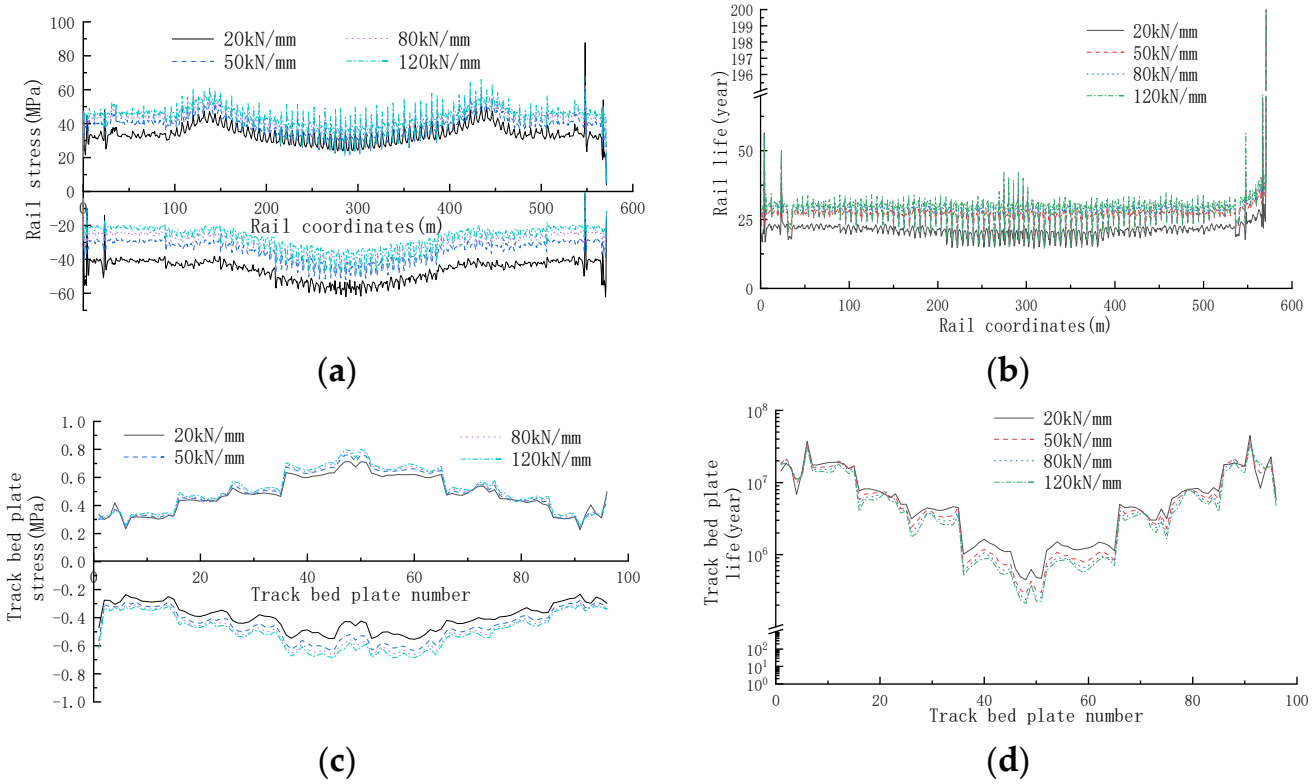

Figure 20. Fatigue characteristics of structures with different fastener vertical stiffness: (**a**) stress envelope diagram of Rail; (**b**) rail fatigue life; (**c**) stress envelope diagram of track bed slab; (**d**) fatigue life of track bed slab.

As Figure 20 shows, with the increase of vertical fastener stiffness, the tensile stress of the rail increases, the compressive stress decreases, and the stress amplitude decreases. The fatigue life of the rail increases from 20.9 years to 29.4 years; The connection between the rail and the track bed slab is continuously strengthened, the tensile and compressive stresses of the track bed slab are increased, and the life of the most unfavorable position of the track bed slab is from 4.4×10^5 years to 2.1×10^5 years. The tensile and compressive stresses and the minimum life of the base plate are essentially unchanged.

6.3. Train Speed

Keep the original design parameters of the structure unchanged. See Figure 21.

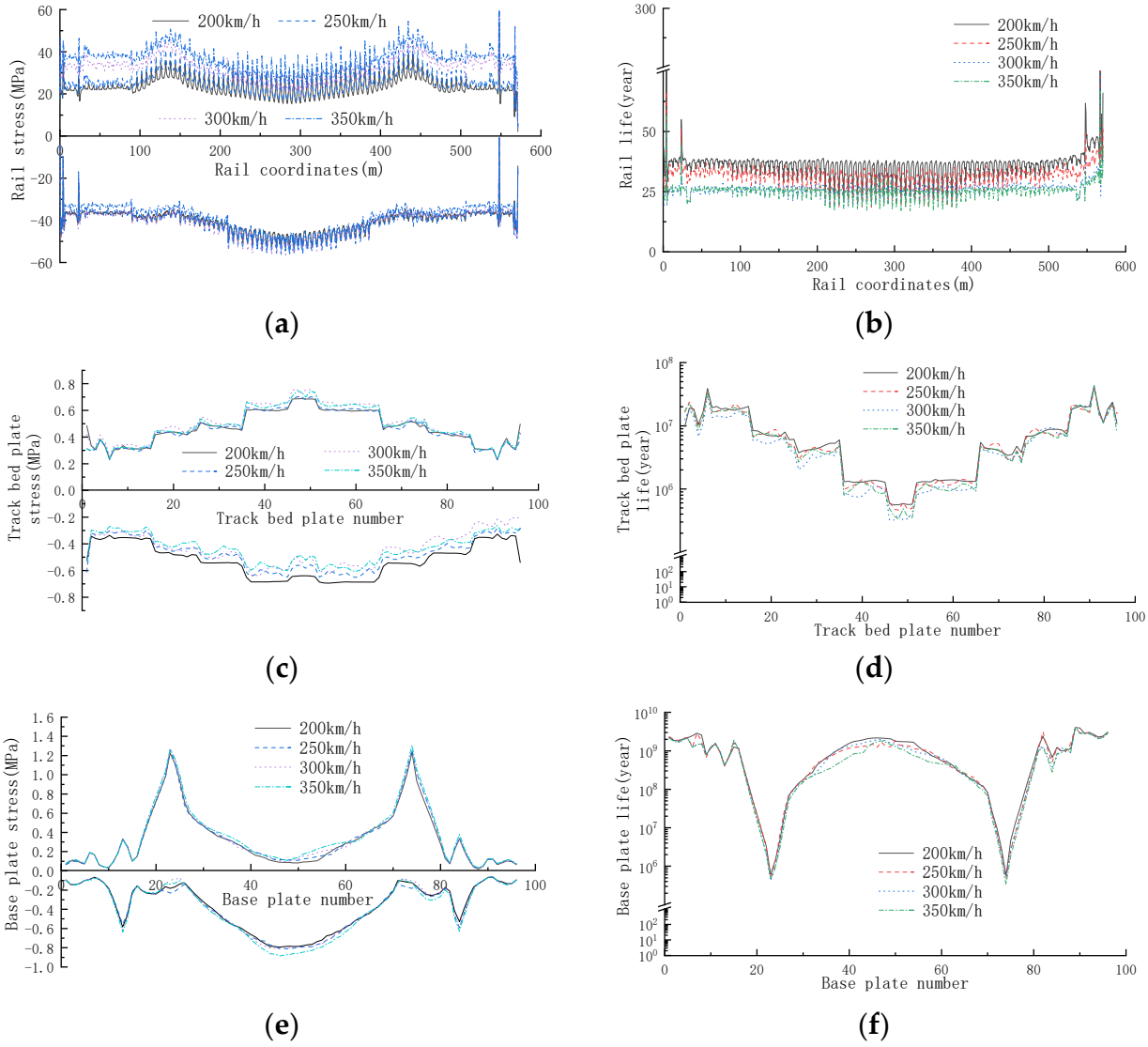

Figure 21. Structural fatigue characteristics under different train speeds: (**a**) Stress Envelope Diagram of Rail; (**b**) Fatigue life of rail; (**c**) Stress envelope diagram of track bed slab; (**d**) Fatigue life of track bed slab; (**e**) Stress envelope diagram of base plate; (**f**) Fatigue life of base plate.

From Figure 21 it can be seen that with the increase of train operation speed, the tensile stress on the rail increases, and the minimum service life of the rail decreases from 35.7 years to 25.3 years; The maximum tensile stress of the track bed slab is continuously increasing, and the combined effect of stress causes the minimum life of the track bed slab to change from 5.5×10^5 years to 3.3×10^5 year. The connection between the base plate and the bridge is strong. The increase of the train speed enhances the dynamic deformation of the bridge. The service life of the base plate at the bridge tower is 5.7×10^5 years reduced to 3.3×10^5 years.

7. Conclusions

Taking a (40 + 64 + 40) m continuous beam on Beijing Shenyang Passenger Dedicated Line and a 300 m composite girder cable-stayed bridge on Chang Gan Passenger Dedicated Line as the research objects, this paper establishes a simulation model of the bridge CRTS I double block ballastless track system by using the finite element method, and studies the longitudinal force distribution rule of the jointless track on the bridge and the dynamic response characteristics of the bridge, track bed plate, base plate and rail under the action

of train live load, combined with Miner's criterion and S-N curve, The fatigue damage rule of ballastless track structure on long-span bridges under train load is discussed, and the influence of changes in elastic cushion stiffness, fastener stiffness and train speed on the fatigue characteristics of ballastless track structure is revealed. The main conclusions are as follows:

(1) For the bridge ballastless track system, under the action of temperature load, the maximum compressive stress of the steel rail expansion force on the simply supported beam and continuous beam is located near the bridge support, and the maximum tensile stress of the steel rail on the simply supported beam, continuous beam and cable-stayed bridge appears in the middle of the bridge span; Under flexure load, the extreme value of tensile stress of rail flexure is located near the bridge support, and the extreme value of compressive stress is located in the middle of the bridge span; Under the action of braking load, the extreme positions of the tensile and compressive stress of the rail braking force on the simple supported beam and continuous beam are located near the bridge support. The maximum tensile stress of the rail on the cable-stayed bridge appears in the middle of the main beam span, and the maximum compressive stress appears near the bridge tower support.

(2) Under the action of train dynamic load, the service life curve of steel rails on simply supported beams, continuous beams and cable-stayed bridges is relatively smooth. Because the structural system of cable-stayed bridges is relatively flexible, the minimum service life of steel rails is reduced from 27.1 years on continuous beams to 17 years on cable-stayed bridges.

(3) Under the action of train dynamic load, the service life curves of rails and track bed plates on simply supported beams and continuous beams are relatively smooth, and the service life is basically the same. The service life curves of track bed plates on cable-stayed bridges are related to the stiffness of elastic cushion, which decreases step by step. Meanwhile, the track bed plates will not be fatigue damaged during the service period. The life curve of the base plate is related to the bridge. The minimum life occurs near the bridge bearing, and the base plate will not be fatigue damaged during the service period.

(4) The fatigue life of track bed slab can be effectively improved by appropriately increasing the stiffness of elastic cushion. Properly increasing the vertical fastener stiffness can enhance the connection between the rail and the track bed slab, and can improve the rail life but reduce the fatigue life of the track bed slab. The increase of train speed will increase the dynamic stress amplitude of track structure and reduce the fatigue life.

The analysis process of the fatigue characteristics of the long-span bridge-double-block ballastless track system is complex, and there are many factors to consider in practice. For the calculation contents and methods studied in this article, there are still many issues that deserve further research, mainly the following aspects:

(1) In practical situations, the nonlinear characteristics and uncertainties of the bridge and track system may affect the accuracy of the model. Therefore, it is necessary to further optimize and improve the analysis model to improve the accuracy and reliability of the research.

(2) Reliability analysis can consider uncertain factors and provide more comprehensive and accurate results for the evaluation of the fatigue characteristics of ballastless track structures. However, this paper lacks research on reliability, and thus future research should consider using reliability analysis to evaluate the service life of ballastless track structures and provide reliability design methods.

(3) This paper only considers the dynamic response characteristics of components such as the bridge, ballast mat, base plate, fasteners, and steel rails, while the effects of external environmental factors such as wind and temperature also play an important role. Future research can further explore the impact of multi-field coupling on the fatigue characteristics of ballastless track structures.

(4) In the study of the fatigue characteristics of the long-span bridge-double-block ballastless track system, continuous beam bridges and cable-stayed bridges are chiefly under consideration. Therefore, the research types of long-span bridges can be expanded.

Author Contributions: Conceptualization, B.Y.; methodology, B.Y.; software, B.Y.; validation, B.Y., J.T. and J.H.; formal analysis, B.Y.; writing—original draft preparation, B.Y., J.T. and J.H.; writing—review and editing, J.T., J.H. and P.L. All authors have read and agreed to the published version of the manuscript.

Funding: This research was funded by the National Natural Science Foundation of China (grant number 52278470) and the Natural Science Foundation of Hunan Province (grant number 2022JJ30741).

Institutional Review Board Statement: Not applicable.

Informed Consent Statement: Not applicable.

Data Availability Statement: All data, models and code generated or used during the study appear in the submitted article.

Acknowledgments: The authors would like to thank the National Natural Science Foundation of China (Project No. 52278470) and the Natural Science Foundation of Hunan Province (Project No. 2022JJ30741).

Conflicts of Interest: The authors declare no conflict of interest.

References

1. Song, Y.; Liu, Z.G.; Ronnquist, A.; Navik, P.; Liu, Z.D. Contact Wire Irregularity Stochastics and Effect on High-Speed Railway Pantograph-Catenary Interactions. *IEEE Trans. Instrum. Meas.* **2020**, *69*, 8196–8206. [CrossRef]
2. Liu, C.; Thompson, D.; Griffin, M.J.; Entezami, M. Effect of train speed and track geometry on the ride comfort in high-speed railways based on ISO 2631-1. *Proc. Inst. Mech. Eng. Part F-J. Rail Rapid Transit* **2020**, *234*, 765–778. [CrossRef]
3. Dai, G.; Ge, H.; Qiu, Y.; Liu, W. Study on stress of broken slab of ballastless track on long-span continuous beam bridge of high-speed railway. *J. Huazhong Univ. Sci. Technol. (Nat. Sci. Ed.)* **2015**, *43*, 100. (In Chinese)
4. Li, Y.; Su, Y.; Xia, F.; Zhang, N. Vertical dynamic response of the ballastless track on long-span plate-truss cable-stayed bridges. *Sci. China-Technol. Sci.* **2015**, *58*, 236–247. [CrossRef]
5. Wenner, M.; Marx, S.; Koca, M. Additional rail stresses due to long-term deformations of railway viaducts with ballastless track—Model and reality. *Bautechnik* **2019**, *96*, 674. [CrossRef]
6. Yan, B.; Gan, R.; Zhang, G.; Zeng, Z. Study on longitudinal force distribution law of jointless track on kilometer level railway suspension bridge. *Railw. Trans.* **2021**, *43*, 130–135. (In Chinese)
7. Xu, Q.; Lin, Q.; Fang, Z.; Zhang, Z. Fatigue characteristics of longitudinal slab ballastless track on bridge under combined load. *China Railw. Sci.* **2017**, *38*, 37. (In Chinese)
8. Zhu, Z.; Feng, Q.; Gong, W.; Yu, Z. Local fatigue analysis of heavy haul railway steel bridge considering vehicle bridge coupling. *J. Railw. Eng.* **2019**, *36*, 36–42, 78. (In Chinese)
9. Li, S.; Yang, R. Study on fatigue life of CRTS-I slab ballastless track. *Railw. Stand. Des.* **2016**, *60*, 34–37. (In Chinese)
10. Shan, Y.; Wang, B.; Zhang, J.; Zhou, S. The influence of dynamic loading and thermal conditions on tram track slab damage resulting from subgrade differential settlement. *Eng. Fail. Anal.* **2021**, *128*, 105610. [CrossRef]
11. Ren, J.; Tian, G.; Xu, J.; Deng, S.; Xie, P. Load action characteristics and fatigue life prediction of passenger freight mixed unit slab ballastless track. *J. Railw.* **2019**, *41*, 110–116. (In Chinese)
12. Poveda, E.; Rena, C.; Lancha, J.; Ruiz, G. A numerical study on the fatigue life design of concrete slabs for railway tracks. *Eng. Struct.* **2015**, *100*, 455–467. [CrossRef]
13. Qu, C. Research on Design Theory and Method of Ballastless Track Jointless Track for High-Speed Railway Long Bridge. Ph.D. Thesis, Beijing Jiaotong University, Beijing, China, 2013; p. 42. (In Chinese)
14. Ren, J. *Design and Maintenance Theory of Ballastless Track on Bridge*; Science Press: Beijing, China, 2015; p. 79. (In Chinese)
15. Liu, Z.; Wen, W.; Chen, L. Design Innovation and Practice of Railway Hybrid Girder Cable stayed Bridge. *J. Railw. Eng.* **2019**, *36*, 30–36. (In Chinese)
16. Yan, B. Study on the Interaction between Medium and Small Span Bridges and Tracks of High-Speed Railway. Ph.D. Thesis, Central South University, Changsha, China, 2013; p. 24. (In Chinese)
17. Zhai, W.; Xia, H. *Theory and Engineering Application of Train Track Bridge Dynamic Interaction*; Science Press: Beijing, China, 2011; p. 174. (In Chinese)
18. Liu, J.; Wei, Q. Fatigue life prediction of high-speed railway rails. *J. Railw. Eng.* **2000**, 30–34. (In Chinese)
19. Gong, J. *Basic Theory and Application of Modern Concrete Structure*; China Architecture Press: Beijing, China, 2009; p. 4. (In Chinese)
20. *TB 10002-2017*; Code for Design of Railway Bridges and Culverts. China Railway Press: Beijing, China, 2017; p. 132. (In Chinese)

21. Yan, B.; Xie, H.; Pan, W.; Dai, G. Dynamic characteristics of train ballastless track bridge system considering track damage. *J. Vib. Eng.* **2020**, *33*, 807–814. (In Chinese)
22. *TB 10082-2017*; Code for Design of Railway Track. China Railway Press: Beijing, China, 2017; p. 26. (In Chinese)
23. *TB 10015-2012*; Code for Design of Railway Seamless Track. China Railway Press: Beijing, China, 2013; p. 59. (In Chinese)